Cell, Vol. 119, 693–705, November 24, 2004, Copyright ©2004 by Cell Press

Circadian Gene Expression in Individual Fibroblasts: Cell-Autonomous and Self-Sustained Oscillators Pass Time to Daughter Cells

Emi Nagoshi,[1] Camille Saini,[1] Christoph Bauer,[2] Thierry Laroche,[1] Felix Naef,[3] and Ueli Schibler[1,*]

[1]Department of Molecular Biology and NCCR Frontiers in Genetics
Sciences III
[2]Imaging Platform
NCCR Frontiers in Genetics Sciences II
University of Geneva
30, Quai Ernest Ansermet
CH-1211 Geneva-4
Switzerland
[3]Computational Systems Biology
ISREC and NCCR Molecular Oncology
Chemin des Boveresses 155
CH-1066 Epalinges
Switzerland

Summary

The mammalian circadian timing system is composed of a central pacemaker in the suprachiasmatic nucleus (SCN) of the brain and subsidiary oscillators in most peripheral cell types. While oscillators in SCN neurons are known to function in a self-sustained fashion, peripheral oscillators have been thought to damp rapidly when disconnected from the control exerted by the SCN. Using two reporter systems, we monitored circadian gene expression in NIH3T3 mouse fibroblasts in real time and in individual cells. In conjunction with mathematical modeling and cell co-culture experiments, these data demonstrated that in vitro cultured fibroblasts harbor self-sustained and cell-autonomous circadian clocks similar to those operative in SCN neurons. Circadian gene expression in fibroblasts continues during cell division, and our experiments unveiled unexpected interactions between the circadian clock and the cell division clock. Specifically, the circadian oscillator gates cytokinesis to defined time windows, and mitosis elicits phase shifts in circadian cycles.

Introduction

The mammalian circadian timing system has a hierarchical structure, in that a master pacemaker in the suprachiasmatic nucleus (SCN) coordinates subsidiary oscillators in most peripheral tissues (Reppert and Weaver, 2002; Schibler and Sassone-Corsi, 2002). Circadian clocks can measure time only approximately and thus have to be synchronized every day to remain in resonance with geophysical time. While the oscillators of SCN neurons are synchronized primarily through photic signals, feeding time appears to be the dominant timing cue (Zeitgeber) for peripheral clocks (Damiola et al., 2000; Stokkan et al., 2001).

*Correspondence: ueli.schibler@molbio.unige.ch

That circadian oscillators exist even in established cell lines could be demonstrated by a serum shock (Balsalobre et al., 1998). Thus, a short incubation of confluent Rat-1 cells with high concentrations of serum elicited several daily cycles of clock gene expression. Subsequently, a bewildering variety of substances were shown to trigger similar circadian cycles of transcript accumulation in cultured cells (Akashi and Nishida, 2000; Balsalobre et al., 2000a, 2000b; Brown et al., 2002; Hirota et al., 2002; Yagita and Okamura, 2000).

Available evidence argues that both master and subsidiary oscillators utilize a very similar clock gene circuitry for rhythm generation (Balsalobre et al., 1998; Yagita et al., 2001). This molecular clockwork involves the transcriptional repressors CRY1, CRY2, PER1, and PER2 and the transcriptional activators BMAL1 and CLOCK. The BMAL1:CLOCK heterodimer activates *Per* and *Cry* transcription and, once PER and CRY proteins reach sufficiently high concentrations, they form nuclear complexes that interfere with BMAL1:CLOCK-mediated transactivation and thereby inhibit transcription of their own genes. This feedback loop mechanism generates circadian oscillations of *Per* and *Cry* expression. The same positive and negative regulatory components also govern the rhythmic expression of *Rev-erb*α, and the circadian accumulation of REV-ERBα results in the periodic repression of *Bmal1* and *Clock*. Thereby, REV-ERBα interconnects the cyclic expression of positive and negative limb members (for review see Reppert and Weaver, 2002).

In spite of the mechanistic similarities between central and peripheral oscillators, it was thought that only the former are self-sustained (Schibler and Sassone-Corsi, 2002; Yamazaki et al., 2000). Individual SCN neurons can generate robust circadian rhythms in electrical firing frequency and clock gene expression with little if any damping for many days (Liu et al., 1997; Welsh et al., 1995; Yamaguchi et al., 2003), but the amplitude of mRNA cycles observed in serum-shocked fibroblasts or tissue explants from animals decreases rapidly over time. We wanted to examine whether this is caused by damping or dephasing of the molecular oscillator. Using two reporter systems, we demonstrate that NIH3T3 fibroblasts possess robust cell-autonomous and self-sustained oscillators whose function even persists during cell division. Moreover, our experiments suggest some unanticipated interactions between cell divisions and circadian oscillations

Results

Circadian Gene Expression in Individual NIH3T3 Fibroblasts

By monitoring the accumulation of mRNA issued by various clock and clock-controlled genes, we have previously shown that a serum shock elicits circadian gene expression in cultured fibroblasts. Populations of untreated cells showed nearly constant expression levels, and we thus considered two mechanism: Serum might

jumpstart damped oscillators or it might synchronize self-sustained but dephased oscillators (Balsalobre et al., 1998). To discriminate between these models, we wished to establish a reporter system that allows the recording of circadian rhythms in individual cells. Hence, we decided to develop a cell line that rhythmically expresses a fluorescent protein. We chose the enhanced YFP derivative Venus as reporter because the fluorescence intensity of Venus is about 10-fold higher than that of GFP and about 30-fold higher than that of YFP. Moreover, Venus has a higher folding efficiency than YFP so that the fluorescence expression follows Venus translation without a large time lag (Nagai et al., 2002). To allow for a large amplitude of cyclic Venus accumulation and to increase the fluorescence density within cells, we engineered a short-lived and nuclear fluorescent protein, dubbed VNP (*V*enus-*N*LS-*P*EST), by fusing DNA sequences encoding a nuclear localization signal and a PEST element to the open reading frame of Venus. In our first attempts, we used *Bmal1* promoter sequences to regulate circadian VNP expression. However, although these regulatory sequences proved successful in driving readily detectable luciferase expression (see below), they failed in expressing VNP levels yielding fluorescence signals that are satisfactory for timelapse microscopy. We thus constructed the Rev-erbα-VNP expression vector depicted in Figure 1A, based on previously gained knowledge that in liver *rev-erbα* is transcribed at an about 20-fold higher rate than *Bmal1* and that the *rev-erbα* sequences contained in this vector drive robust circadian transcription in transgenic mice (Preitner et al., 2002). A stably transformed clonal cell line, NIH3T3-Rev-VNP-1, that yielded readily detectable nuclear fluorescence in more than 50% of the cells was selected. To examine whether Rev-VNP-1 cells display circadian rhythms, we grew cells to confluence, stimulated them with 50% horse serum, and continuously recorded fluorescence by timelapse microscopy during three consecutive days in medium containing 0.5% serum. As seen in the timelapse video recording provided in Supplemental Data (Supplemental Movie S1 at http://www.cell.com/cgi/content/full/119/5/693/DC1/), robust and nearly synchronous circadian rhythms of nuclear VNP fluorescence were observed in many individual NIH3T3 fibroblasts. A fluorescence recording of a single nucleus is presented in Figure 1B, and circadian fluorescence profiles are depicted in Figures 1C and 1D. As illustrated in Figure 1D, VNP expression levels varied greatly between individual cells, and the minimum intensities recorded for some cells were similar to the maximal intensities observed in other cells. This explains why VNP fluorescence could not be recorded in 100% of NIH3T3-Rev-VNP-1 cells. Interestingly, in spite of these uneven fluorescence levels, the daily oscillations in individual cells were roughly synchronous after the serum treatment. The timelapse movie (Supplemental Movie S1) displayed online indicates that many cells died after two circadian cycles. At least in part, this accelerated cell death may have resulted from repeated fluorescence excitation during the recording period.

The timelapse microscopy recordings allowed us to determine the period length (τ) of circadian oscillations in single cells. The histogram depicted in Figure 1E indicates that the distribution of τ is following a Gaussian distribution with a mean value of about 28 hr and a sigma of about 2.9. We noticed that the period length depends on the serum concentration and is approximately 25 hr in media containing serum concentrations of 5% and higher.

We wished to determine whether cells not exposed to a serum treatment also display cyclic VNP accumulation. Before the timelapse recording was initiated, NIH3T3-Rev-VNP-1 cells were seeded at a low density into a culture dish and kept for 60 hr under constant conditions in the incubation chamber of the microscope. The fluorescence profiles of single nuclei (Figures 2A and 2B) show that individual cells displayed robust but out-of-phase circadian VNP accumulation. This observation implies that serum can synchronize detuned individual rhythms and does not initiate de novo rhythms from dormant oscillators.

NIH3T3 Circadian Oscillators Are Self-Sustained

The fluorescence recordings in single cells presented above strongly suggest that NIH3T3 cells are capable of generating self-sustained circadian rhythms of gene expression. This technology also has two drawbacks, however. First, due to the sensitivity of NIH3T3 cells to irradiation (fluorescence excitation), it does not permit recording periods longer than about three days (see Supplemental Movie S1 on the *Cell* website). Secondly, as fluorescence recordings are labor intensive and semiquantitative, it is difficult to establish long-term gene expression profiles for entire cell populations. We thus wanted to scrutinize the conclusions derived on the basis of single-cell fluorescence recordings by real-time bioluminescence recordings, a technology that has been used successfully for the monitoring of circadian gene expression in a variety of systems, including mammalian tissues (Yamazaki et al., 2000; Yoo et al., 2004). To this end, we generated a transgenic cell line, NIH3T3-Bmal1-Luc-1, that expresses a short-lived luciferase transcript from the *Bmal1* promoter (Figure 3A). As shown in Figure 3B, a serum shock elicits robust circadian bioluminescence rhythms. Noticeably, the amplitude (peak/trough ratio) progressively decreased to reach a nonzero steady value after about 10 days, extending until the end of the 19-day recording. A logarithmic representation of the same data (insert of Figure 3B) suggests a precise exponential loss in overall bioluminescence ($T_{1/2} = 3.2$ days), and cell loss appears to be the major cause for the diminishing luminescence (unpublished data). To allow comparison with mathematical models, the data were detrended for exponential decay (Figure 3C) and band pass-filtered (Figures 3D to 3F) to remove a residual infradian component. In principle, the progressive decrease in amplitude observed in Figures 3B to 3F could be caused by *damping* (progressive loss of amplitude in each individual oscillator), *dephasing* (due to different frequencies of individual oscillators), or both *damping and dephasing*. In what follows, we solved these models for an infinite number of cells (the finite population case is mathematically difficult) and for each scenario, we fitted the predicted envelope, defined as the line passing through the peaks and troughs, to the experimental data (for details see Figure 3 legend and Experimental Procedures). Close fits were

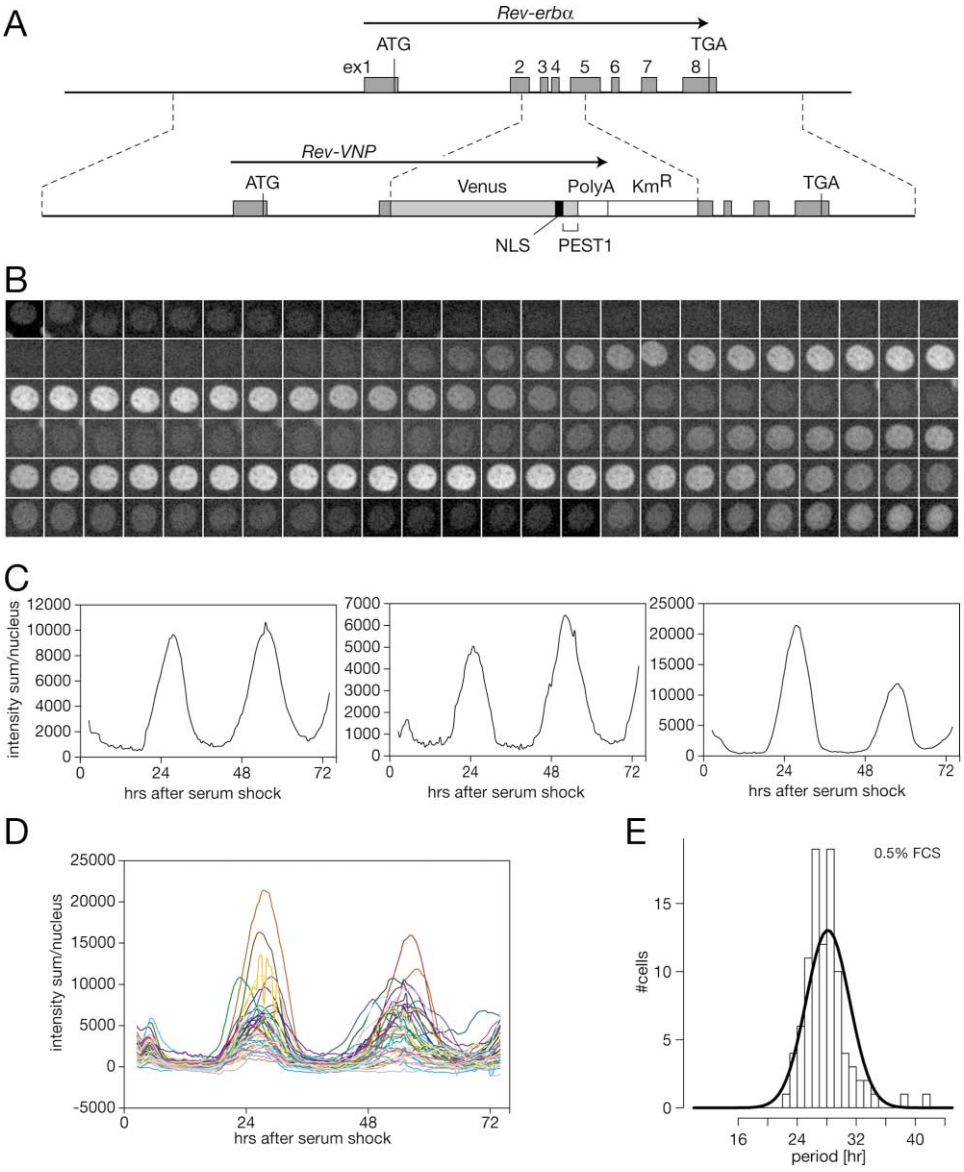

Figure 1. The Recording of Circadian Gene Expression in Individual NIH3T3 Fibroblasts

(A) Schematic structure of the circadian reporter gene expressed in the NIH3T3-Rev-VNP-1 cell line (for details, see Experimental Procedures). The VNP (*V*enus-*N*LS-*P*EST) fluorescent protein accumulates in the nucleus and is short lived since it contains a nuclear localization signal from Simian Virus 40 large T-antigen and a PEST sequence from the mouse ornithine decarboxylase gene.

(B) Timelapse microscopy of circadian VNP fluorescence in the nucleus of an individual cell after a serum shock. Images were taken every 30 min during three consecutive days.

(C) Circadian fluorescence profiles of nuclei from three individual cells after a serum shock. For each graph, the fluorescence intensity over the nucleus was quantified (see Experimental Procedures) and plotted against time.

(D) Circadian fluorescence profiles of 42 individual cell nuclei after a serum shock. Note that the signal magnitudes vary dramatically between different cells.

(E) Histogram of periods (time span between two fluorescence peaks of individual cells grown in DMEM containing 0.5% FCS after the serum shock); the density (fat solid line across histogram) is obtained from a best fit to a Gaussian distribution (mean = 28.2 hr, SD = 2.9 hr).

obtained with the envelopes generated by the *pure dephasing* model (Figure 3E) and the *damping+dephasing* model (Figure 3F). Not surprisingly, the *pure damping* model provided the least accurate fit to the experimental curve. This model would actually demand that all cellular oscillators contributing to the compound bioluminescence wave have an identical period length, a postulate that is untenable based on the single cell recordings presented above. We thus speculate that the dephasing of detuned oscillators was the major cause for the loss of amplitude in our bioluminescence recording and that the damping of individual oscillators probably contributed little to this trend. Our mathematical simulations, which are based on infinite populations, predict that the amplitude approaches zero in all three models after extended time periods (Figures 3D–3F). For the *pure*

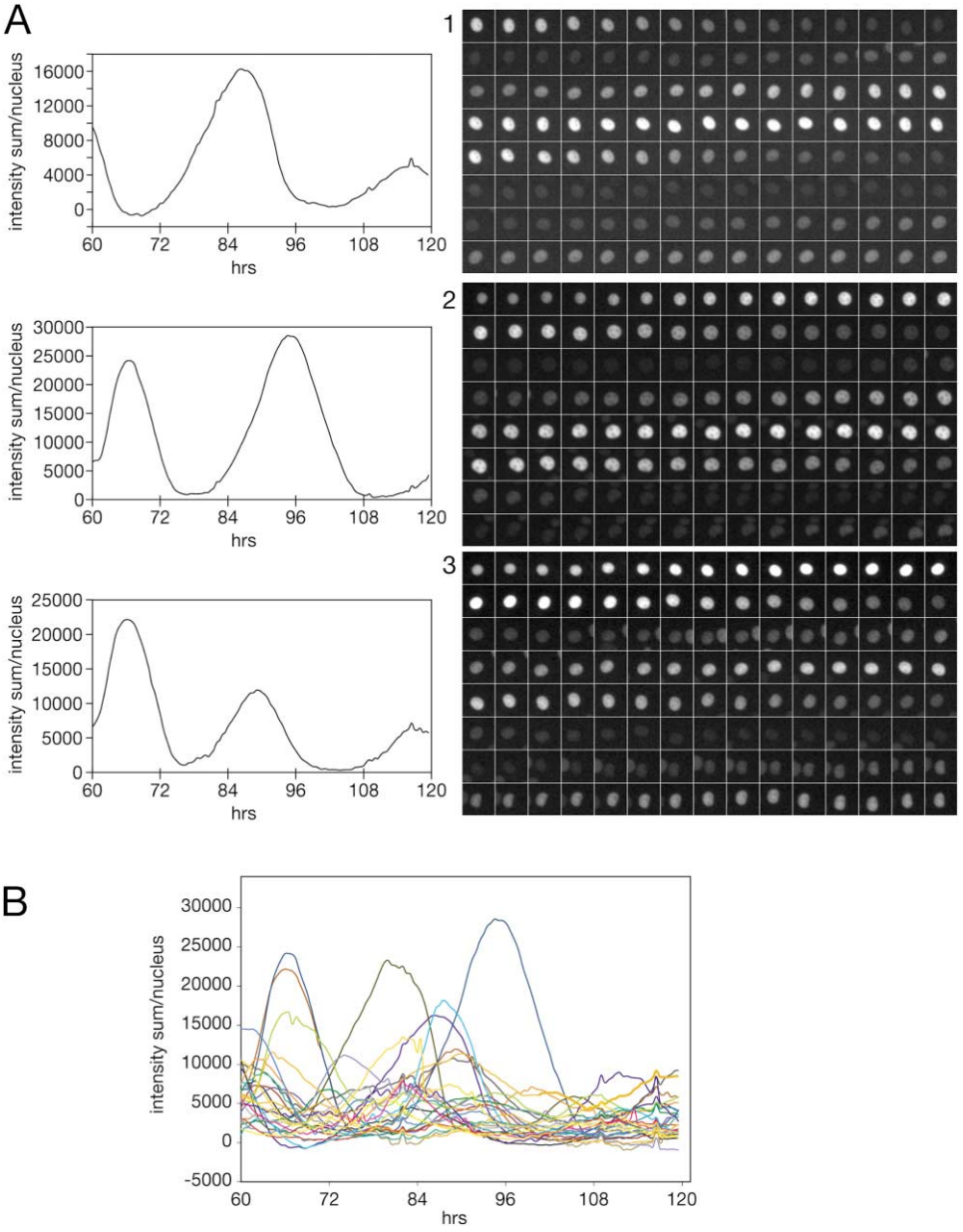

Figure 2. Circadian Rhythms Are Desynchronized in Untreated Individual NIH3T3 Cells

Cells were grown in DMEM containing 20% serum to near confluence before timelapse microscopy was initiated. Recording and analysis of fluorescence was performed as in Figure 1.

(A) Fluorescence recordings of three individual cells. The fluorescence profile for each cell is given to the left of the micrograph assemblies. Note that the three cells have widely different phases.

(B) Circadian fluorescence profiles of 26 individual cells. Note that the circadian cycles of individual cells are not (or poorly) synchronized.

damping model, the number of oscillators does not affect the simulated compound profile since all oscillators have identical frequencies (Figure 3G). However, the simulation of populations composed of finite numbers of detuned oscillators yielded an unexpected outcome after extended time periods. For example, for a population of 5000 individual oscillators, small amplitude oscillations persist indefinitely (Figure 3H). We estimate that the number of live cells between 12 and 19 days of recording was between 15,000 and 3,000. For geometrical reasons of photon counting, the 5000 detuned oscillators used for the simulations in Figures 3G and 3H is probably an upper bound for the number of cells contributing to the bioluminescence profile during the last 7 days of the recording. As predicted by the dephasing model for a limited number of oscillators (Figure 3H), the bioluminescence profile displays low-amplitude but persistent oscillations after about 10 days of recording.

In summary, our analysis suggests that the dephasing of detuned oscillators was the major cause for the loss of amplitude in our bioluminescence recording and that damping of individual oscillators contributed little to the

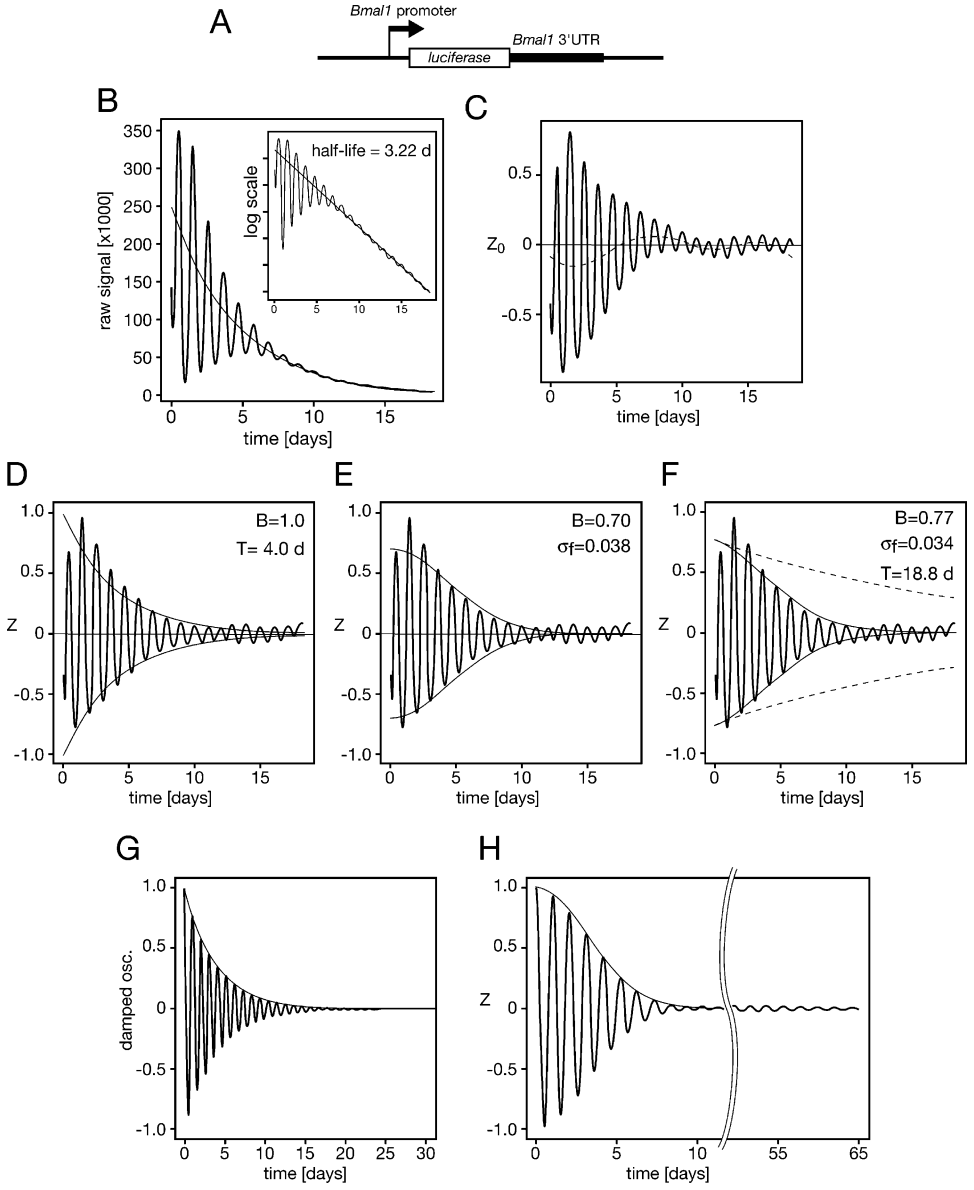

Figure 3. Persistent Circadian Expression of Luciferase by NIH3T3 Fibroblasts

(A) Schematic structure of the circadian reporter gene expressed in the NIH3T3-Bmal1-Luc-1 cell line.

(B) NIH3T3-Bmal1-Luc-1 cells were grown to confluence and serum-shocked. Bioluminescence was then recorded as 1 min photon count bins for 19 consecutive days. The cells were kept in medium containing 10% FCS during the recording period. Insert: on a logarithmic scale, the exponential decay attributed to cell loss is clearly visible. Regression analysis (line across the peaks) estimates a half-life of 3.22 days.

(C) The raw data shown in the insert of panel B were detrended for cell loss (see Experimental Procedures). The dotted line shows a residual slow component (periods $>$ 4.6 days) detected by using a low-pass filter. This infradian component was eliminated in (D)–(F).

(D–F) Comparison with mathematical models. Z, the modeled quantity, is equal to Z_0 minus the slow component from (C). We modeled populations with infinite numbers of oscillators and thus constrained the fits to times less than 10 days. For longer times, we have no reason to expect the model envelopes to describe the data (see text and [H] and [G]). (D) Model for tuned (equal frequency) damped oscillators (*pure damping* model). (E) Detuned (unequal frequencies), sustained (nondamped) oscillators (*pure dephasing* model).

(F) Model combining both detuning and damping (*damping+dephasing* model). In each, the predicted envelope for infinite populations (solid lines) is fit to the peaks and troughs for times shorter than 10 days (so that the finite population effects are small, cf. [G]) using polynomial regression. Differences in model predictions are subtle and can be seen best in the shape of the envelope near t $=$ 0: (D) starts linear, (E) starts purely quadratic, and (F) has linear and quadratic terms. (F) is very similar to (E), indicating that detuning is the dominant effect. Mean frequency is estimated to 24.5 hr so that the relative values indicated for σ_f translate to 0.93 (E) and 0.83 (F) hrs.

(G) Simulation of damping oscillators with a damping time t $=$ 4 days (see model definition in Experimental Procedures). Damping oscillations, as indicated by their name, progressively diminish their amplitude over time and vanish after about 30 days. Since the *pure damping* model requires that all oscillators have an identical period length, the shape of the profile does not depend on the number of oscillators.

(H) Finite populations explain the residual oscillations observed at long times. Simulation for 5000 cells with a frequency dispersion of 5% show that short-time envelope follows infinite result up to $\sim$10 days, but residual oscillations continue indefinitely, as seen in the 50–60 days window. (E) and (F) are therefore compatible with long-time residual oscillations, even though their infinite size behavior predicts vanishing oscillations after $\sim$12 days.

observed trend. Hence, these compound recordings support the conclusions drawn on the basis of our single-cell fluorescence recordings presented in Figures 1 and 2.

A Single Phase-Shifting Pulse Can Synchronize All Phases of Circadian Fibroblast Clocks

The synchronization model posits that a single stimulus can reset all possible phases in a population of oscillators to the same phase. To examine this prediction formally, confluent NIH3T3-Bmal1-Luc-1 cells were serum shocked, and parallel cultures were treated with short pulses of dexamethasone at different times during the second bioluminescence cycle. We used dexamethasone in these experiments since pulses of 15 min are sufficient to induce circadian rhythms in cultured cells. This enabled us to establish a phase response curve with high temporal resolution. Four examples of phase-shifted luciferase waves are presented in Figure 4A, and the data obtained for all time points are summarized in the phase shift response (PRC) and phase transition (PTC) curves displayed in Figures 4B and 4C, respectively. The phase response curve (Figure 4B), in which the magnitude of the phase shift was plotted against circadian time, shows that phase shifts could reach maximal possible values of $\pm$12 hr at certain circadian times. When the new phase is plotted against the old phase (Figure 4C), the slope of the phase transition curve is close to zero, indicating that a strong phase-shifting agent can reset oscillations of every conceivable phase to the same phase. This phase response—qualified as type zero in chronobiological parlance—is in stark contrast to the type one phase response observed for light-induced phase shifts of circadian behavior in laboratory rodents.

Fibroblast Oscillators Are Not Influenced by the Circadian Properties of Neighboring Cells

Although all experiments presented thus far are consistent with a cell-autonomous function of fibroblast circadian oscillators, we wished to examine by a more rigorous approach whether signaling between neighboring cells plays a role in circadian rhythm generation. If so, one would expect that paracrine signaling molecules secreted by one cell would impart on the rhythm of its neighbors. As a consequence, cells with nonresonant clocks might either interfere with each others' rhythms or integrate their oscillations to yield an intermediate output, as demonstrated for SCN neurons of mouse chimeras composed of wild-type and *Clock* mutant cells (Low-Zeddies and Takahashi, 2001). We performed a series of co-culture experiments in which NIH3T3-Bmal1-Luc-1 reporter cells were mixed with a 20-fold excess of nonluminescent feeder cells having different circadian properties (Figure 5A). After the mixed cells had reached confluence, their oscillators were synchronized by a serum shock, and the bioluminescence cycles of NIH3T3-Bmal1-Luc-1 cells were recorded. In the first experiment we used Rat-1 fibroblast as feeder cells because we had noticed that Rat-1 cells and NIH3T3 cells started rhythms from different phases (Rat-1 rhythms are advanced by 6 hr with regard to NIH3T3 cells) even when stimulated by the same method (dotted line in Figure 5B). Yet, there was no difference in phase and period length of luciferase rhythms between NIH3T3-Bmal1-Luc-1 cells mixed with either Rat-1 or NIH3T3 feeder cells. Work by Sassone-Corsi and coworkers (Pando et al., 2002) has suggested that mouse embryonic fibroblasts (MEFs) from *mPer*1 knockout mice have significantly shorter periods (20 hr) than MEFs from wild-type mice, and using lentiviral Bmal1-Luc expression vectors, our group has confirmed this difference (S.A. Brown and U.S., unpublished data). We thus compared luminescence rhythms of NIH3T3-Bmal1-Luc-1 cells co-cultured with either wild-type or *mPer1*-deficient MEFs and found once more that the feeder cells did not influence luminescence cycles generated by NIH3T3-Bmal1-Luc-1 reporter cells (Figure 5C). Finally, we used primary fibroblasts from *mPer1/mPer2* double knockout mice as feeder cells that are incapable of circadian rhythm generation. Again, the bioluminescence cycles were very similar to those produced by NIH3T3-Bmal1-Luc-1 surrounded by primary fibroblasts from adult wild-type mice (Figure 5D).

All in all, the results presented in this section strongly suggest that NIH3T3 cells do not communicate with each other with regard to circadian rhythm generation. However, we did not yet determine whether these cells respond to systemic Zeitgeber cues produced in intact animals, as has been demonstrated for mouse embryonic fibroblasts (Pando et al., 2002).

Circadian Gene Expression Persists in Dividing Cells

In the experiments with confluent cells presented thus far, the cells were probably arrested in the G_0 phase of the cell cycle. To the best of our knowledge, circadian gene expression has never been monitored in proliferating cells in culture. We thus wished to examine whether actively dividing cells are also capable of generating daily cycles of gene expression, and if so, whether the circadian oscillator and the cell division clock interact with each other. In a control experiment with confluent NIH3T3-Bmal1-Luc-1 cells, we found that a brief treatment with dexamethasone induces robust circadian rhythms in cells cultured in medium containing 5% to 20% serum (Figure 6A). We thus applied this synchronization method to proliferating NIH3T3-Bmal1-Luc-1 cells plated at a low density in media containing different concentrations of serum (5%, 10%, and 20%). As shown in Figure 6B, sustained circadian oscillations of bioluminescence were observed throughout the 7-day recording period, and as expected, the luminescence signals rose with increasing cell number. In the media containing 5%, 10%, and 20% serum, the average population doubling times of NIH3T3-Bmal1-Luc-1 cells were estimated to be 60 hr, 34 hr, and 28 hr, respectively, during the first 4 days of the recording. We concluded from these experiments that cell division does not abolish the generation of circadian cycles.

To monitor circadian gene expression in individual dividing cells, we plated NIH3T3-Rev-VNP-1 cells at a low density in medium containing 20% FCS, shocked them with dexamethasone as outlined above for NIH3T3-Bmal1-Luc-1 cells, and recorded their fluorescence by timelapse microscopy. Images were again acquired ev-

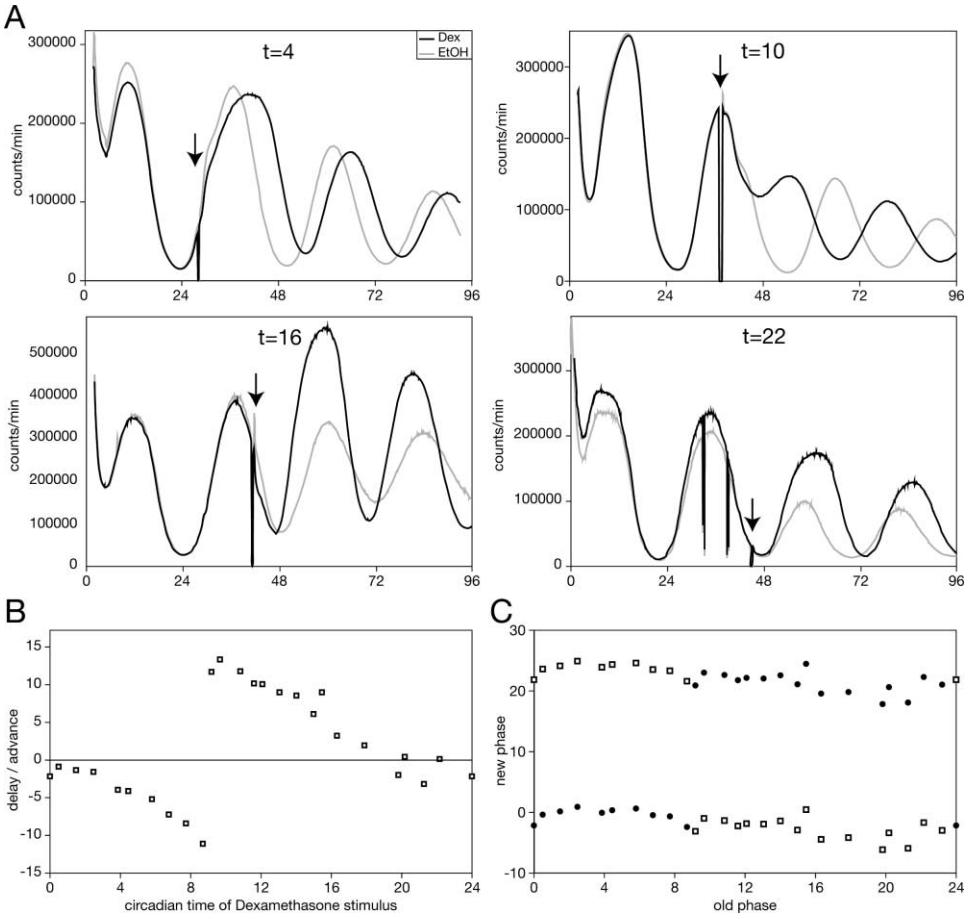

Figure 4. A Single Pulse of Dexamethasone Can Reset All Phases in NIH3T3 Cells

(A) NIH3T3-Bmal1-Luc-1 cells were serum-shocked at time 0. At the indicated circadian times (4, 10, 16, 22, during the second luminescence cycle), parallel cultures were treated for 15 min with 100 nM dexamethasone (black curves) or with the solvent (ethanol) alone (gray curves, control). The dexamethasone stock was 10 mM in 100% ethanol, and the final ethanol concentration in dexamethasone treated and untreated cells was thus 0.001%. Circadian time 0 is defined as the time at which the minimal bioluminescence was observed (around 24 hr). Circadian time is corrected for the period length of luminescence cycles generated by solvent-treated (control) NIH3T3-Bmal1-Luc-1 cells.

(B) Phase response curve (PRC). Dexamethasone pulses were applied to parallel cultures approximately every hour as described in (A). The resulting phase shifts, corrected for the small phase shifts obtained with solvent alone (see [A]), were plotted against circadian time.

(C) Phase transition curve. The data presented in (B) are represented as a phase transition curve (PTC), in which the new phase is plotted against the old phase. Black dots and open squares can be considered as phase shifts measured on two consecutive days. For simplicity all points are plotted on both days. Note that all new phases are nearly identical irrespective of when cells were treated with dexamethasone. Hence the slope of the PTC is near zero, and the corresponding phase response curve is called type-zero PRC.

ery 30 min to record the accumulation of VNP during cell division. Timelapse imaging clearly reveals that daughter cells resumed the rhythms of mother cells after mitosis (Figure 6C, Supplemental Figure S1, and Supplemental Movie S2). In panel A of Supplemental Figure S1, we present the recording of cells that underwent three divisions during the 72-hr recording period and provide the corresponding tracings of the mother cell and two daughter cells.

The Circadian Clock Gates Cell Division Timing to Distinct Time Windows

To examine whether the circadian clock might influence cell division, we quantified fluorescence recordings from dividing cells and determined the time of cytokinesis relative to circadian VNP accumulation (see examples in panel A of Supplemental Figure S1 online). We then plotted the time of cytokinesis of cells dividing during the second VNP fluorescence cycle against the phase of this cycle, and each VNP cycle length (time between the second and third fluorescence peak) was normalized to 24 hr for every dividing cell. A statistical analysis of the data (Figure 6E) revealed that the frequency distribution is highly nonrandom and that it is best described by three subpopulations with peaks at around 6 hr, 12 hr, and 19 hr relative to the peak of Rev-VNP accumulation. As this trimodal frequency distribution could not be resolved with the uncorrected division times shown in Figure 6D, we feel confident that it indeed reflects a gating by the circadian clock. In a parallel control experiment, the composition of the cell populations was examined by fluorescence-activated cell sorting (FACS). This analysis revealed that the composition of G1 cells, S phase cells, and G2+M phase cells did not vary dramatically during the time between the second and third

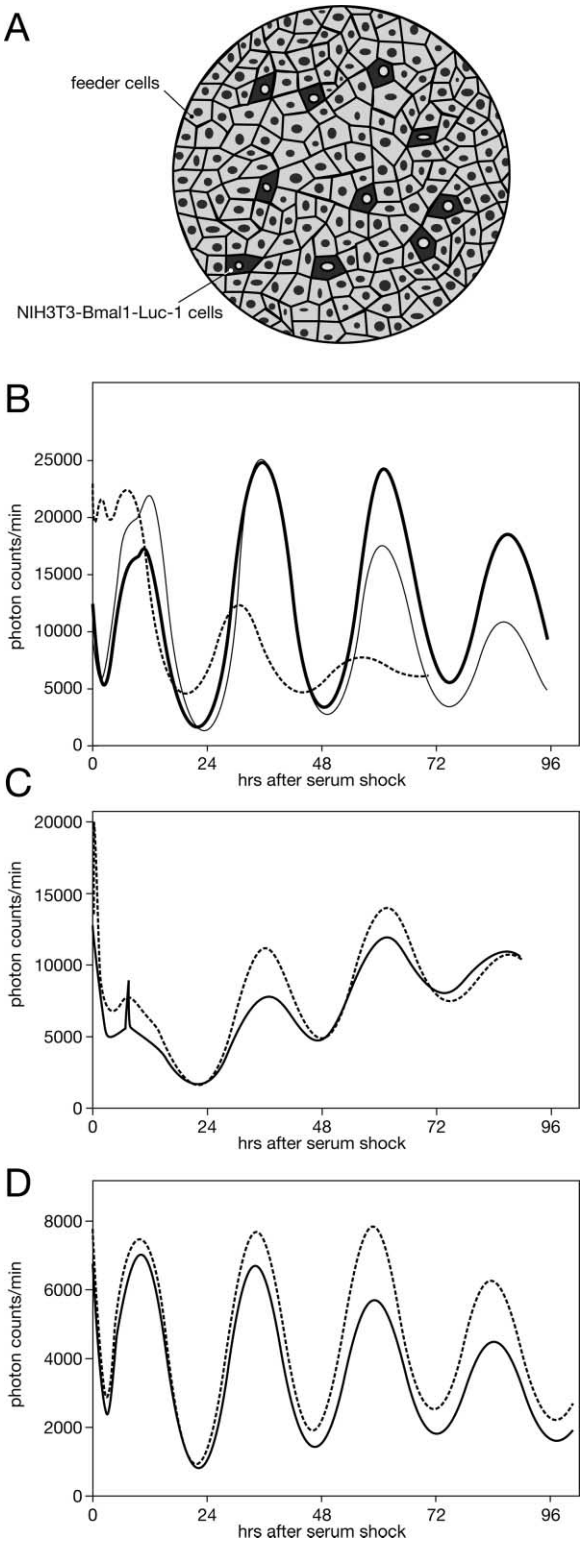

Figure 5. Fibroblast Circadian Oscillators Do Not Communicate with Each Other

(A) Schematic representation of cell co-culture experiments. NIH3T3-Bmal1-Luc-1 reporter cells were mixed with an approximately 20-fold excess of nonluminescent feeder cells. Hence, most reporter cells were surrounded by feeder cells. When the cells reached near confluence, they were serum-shocked, and the bioluminescence of NIH3T3-Bmal1-Luc-1 cells was recorded.

fluorescence peak and hence that cell cycle progression was not synchronized by the dexamethasone treatment during this time window (see Supplemental Figure S2 on the *Cell* website).

The Duration of Circadian Cycles Is Influenced by the Time of Cell Division

We determined the distribution of period lengths for individual proliferating NIH3T3-Rev-VNP-1 cells (Figure 7A) and noticed that it is considerably wider than that measured for nonproliferating cells (Figure 1E). This wider period length distribution manifests itself in a less efficient synchronization (Supplemental Figure S1B), and it may also explain the lower amplitudes recorded for the compound bioluminescence cycles of proliferating cells (Figure 6B) as compared to those obtained for confluent NIH3T3-Bmal1-Luc-1 cells (Figure 6A). To investigate the influence of cell division on period length, we examined whether the circadian time at which a cell divided had an impact on the length of the circadian interval between Rev-VNP peaks occurring immediately before and after division. We selected timelapse recordings for individual cells that divided only once between two peaks of circadian VNP accumulation and plotted the length of the following VNP fluorescence cycle against the time at which the cell divided (Figure 7B). Due to the variability between individual cells, there is considerable scatter of period length throughout the 24 hr cycle. However, the solid line, obtained through a local linear regression, suggests that cell division causes positive and negative phase shifts. The number of recorded cells was not high enough to establish a contiguous phase response curve, but it was sufficient to separate the population into two subpopulations with statistically highly different average VNP cycle length (Figures 7B–7D). Below we offer a plausible interpretation for the correlation between cycle length and cell division time.

Discussion

The Properties of Fibroblast Circadian Oscillators

The results presented in this paper demonstrate that cultured NIH3T3 fibroblasts harbor cell-autonomous and self-sustained circadian oscillators. This conclusion is based on the recording of fluorescence rhythms in single cells and on the mathematical analysis of bioluminescence cycles produced by cell populations. The circadian oscillators of fibroblasts have a relatively wide distribution of period length, and they are therefore not in resonance under normal culture conditions. However,

(B) Feeder cells were NIH3T3 cells (thin solid line) and Rat-1 cells (fat solid line). The dotted curve shows an independent bioluminescence recording of a Rat-1-Bmal1-Luc cell line. Note that the phase of the bioluminescence profile is considerably advanced when compared to that of the NIH3T3-Bmal1-Luc-1 cell line.

(C) Feeder cells were mouse embryonic fibroblasts (MEFs) from wild-type mice (solid line) and *mPer1*$^{-/-}$ mice (dotted line). The MEFs of the *mPer1*$^{-/-}$ mice generate bioluminescence cycles with a 4 hr shorter period than wild-type MEFs (see text).

(D) Feeder cells were primary ear fibroblasts from adult arrhythmic *mPer1*$^{-/-}$; *mPer2*$^{-/-}$ mice (dotted line) and wild-type mice (solid line).

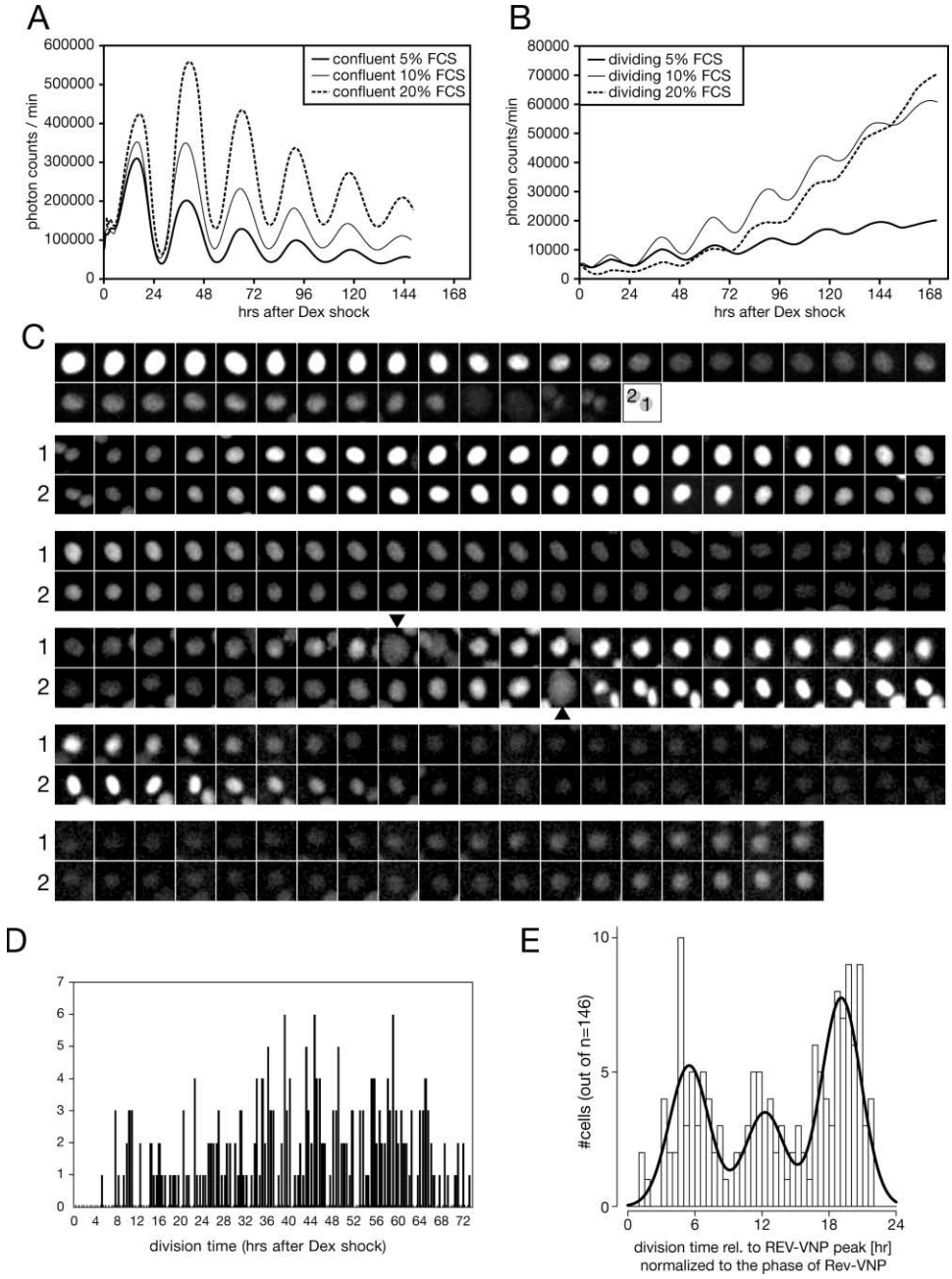

Figure 6. Circadian Gene Expression Persists in Dividing NIH3T3 Fibroblasts

Confluent (A) and proliferating NIH3T3-Bmal1-Luc cells (B) were grown in 5%, 10%, or 20% fetal calf serum (FCS) and circadian gene expression was synchronized by a short dexamethasone (Dex) treatment as in Figure 4. During the first 4 days, the average generation times of proliferating cells were 28 hr in 20% FCS, 34 hr in 10% serum, and 60 hr in 5% serum.

(C) Timelapse microscopy of a dividing NIH3T3-Rev-VNP-1 cell. Images were taken every 30 min. After 16 hr, the mother cell (top line) divided into the daughter cells 1 and 2 (shown schematically in drawing after frame 36). The two circadian fluorescence cycles following cell division are then shown individually for each of the two daughter cells 1 and 2. Both daughter cells divided once more (see arrowheads), but only one of the resulting daughter cells is shown for the remaining recording period.

(D) Frequency of cell division (cytokinesis) after the dexamethasone shock. X-axis: Time in 30-min bins after the dexamethasone shock; Y-axis: number of cells dividing within a 30-min bin ($n = 243$).

(E) Division time histogram relative to Rev-VNP peak. The cell division times of cells that divided between 24 hr and 60 hr after the dexamethasone shock were plotted relative to the phase of the VNP fluorescence cycle. Best fit was obtained for a three component, equal variance Gaussian mixture model with means 5.5, 12.3, 19.1 hr and SD = 1.8 hr. Several independent model selection criteria (BIC, bootstrap parameter estimates, log-likelihood ratio test, cf. Experimental Procedures) were applied and all favored the three-component model unambiguously (not shown).

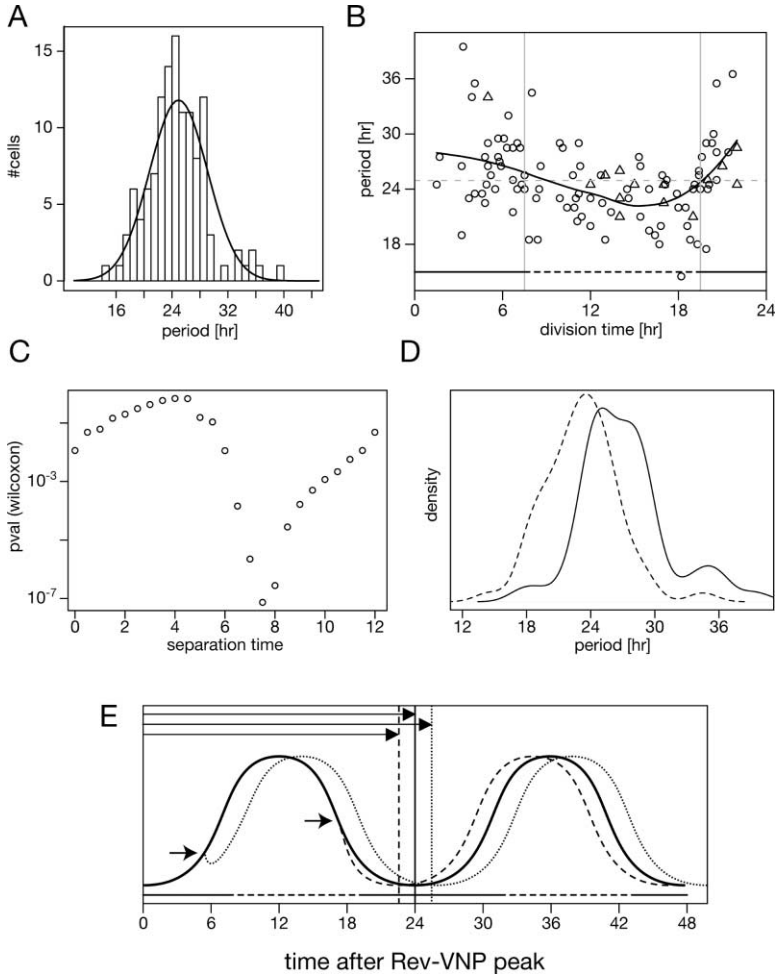

Figure 7. Cell Division Time Influences the Duration of the Following Circadian Cycle

(A) Period histogram for dividing cells grown in DMEM + 20% FCS. Density (solid line) was obtained from a best fit to a Gaussian distribution (mean = 24.9 hr, SD = 4.2 hr).

(B) Peak-to-peak interval around cytokinesis (circadian cycle length) versus time of cytokinesis (rel. to Rev-VNP peak) for two independent experiments (circles and triangles) with cells grown in DMEM + 20% FCS. The solid black line was obtained using a locally linear regression. Significance of the observed trend was assessed by defining two 12 hr windows (horizontal solid and dotted lines) and sliding the boundary between 0 and 12 hr. The two populations show strongest average difference in peak-to-peak duration for a separation time near 7.5 hr (C and D). To verify that significance was not simply the consequence of the large number of separations tested, 10^4 random re-assignments of division times indicated that such level of separation was significant ($p < 10^{-4}$).

(C) p value (Wilcoxon test) profile as function of separation time.

(D) The two populations derived in (B) and (C) have shifted peak-to-peak distributions.

(E) Hypothetical model explaining how cell division can influence the following circadian cycle. For explanation, see text. The fat solid curve mimics the circadian accumulation of CRY:PER complexes, which is antiphasic to REV-ERBα accumulation.

they can be synchronized transiently by a short treatment with substances that activate a wide variety of signaling pathways, and circadian oscillations can be observed in the population for many days. Recently, daily bioluminescence cycles lasting at least 20 days have also been recorded in lung and liver explants from a transgenic mouse expressing luciferase from the *mPer2* locus (Yoo et al., 2004). Hence, peripheral tissues also contain self-sustained oscillators that resemble the ones of NIH3T3 fibroblasts studied in this paper.

Are Peripheral Oscillators Coupled?

The existence of self-sustained and cell-autonomous mammalian oscillators has previously been demonstrated for SCN neurons by recording electrical firing frequency or clock gene expression in individual cells (Liu et al., 1997; Welsh et al., 1995; Yamaguchi et al., 2003). Similar to our findings with NIH3T3 fibroblasts, the period lengths of individual SCN neurons follow a Gaussian distribution with an unexpectedly high sigma (Liu et al., 1997). Clearly, such SCN oscillators must be coupled in the intact animals since otherwise they would rapidly lose synchrony under constant conditions and could therefore not drive coordinated rhythmic outputs of the circadian timing system (Liu et al., 1997). By analyzing the circadian behavior of mouse chimeras whose SCNs were composed of wild-type and homozygous *Clock* mutant cells, Low-Zeddies and Takahashi (2001) have provided direct and compelling evidence for such a coupling mechanism. In these experiments, the circadian phenotypes of chimeras depended on the proportions of wild-type and mutant cells and were clearly intermediate between those observed with wild-type or homozygous Clock mutant mice. Genetic loss-of-function experiments suggest that the VIP/PACAP receptor VPAC2 (Harmar et al., 2002) and the cell adhesion molecule NCAM-180 (Shen et al., 1997) may participate in the paracrine signaling involved in such intercellular coupling.

Our single cell recordings and cell co-culture experiments strongly indicate that cultured fibroblasts do not influence each other's rhythms to any measurable degree. A similar conclusion has recently been reached for cyanobacteria, which also contain self-sustained, cell-autonomous circadian oscillators (Mihalcescu et al., 2004). However, it is possible that paracrine signaling between cells can function only in three-dimensional tissues. As shown by Takahashi and coworkers, different tissue explants harvested from the same SCN-lesioned animal display circadian oscillations with differ-

ent phases and period lengths (Yoo et al., 2004), an observation that would be difficult to interpret without intercellular communication within an organ.

Entrainment Properties of Peripheral Circadian Clocks

We have recorded a high-resolution PRC for circadian NIH3T3 oscillators. As expected on the basis of the synchronization model suggested by our single-cell recordings, a strong chemical stimulus can cause phase shifts of up to 12 hr, and the "new phase" is always similar, irrespective of when the stimulus was applied during the "old phase." This type zero PRC is radically different from the type one PRC recorded for the circadian locomotor activity of laboratory rodents kept in constant darkness and exposed to short light pulses. In this case, phase delays and advances of maximally 2 to 3 hr can be obtained during the first and second half, respectively, of the subjective night, and virtually no phase shifts are elicited by light pulses applied during the subjective day (Daan and Pittendrigh, 1976). The type zero phase response of peripheral oscillators may be biologically relevant, as large phase shifts of up to 8 hr can be observed in vivo under certain food-entrainment conditions (Le Minh et al., 2001).

Interaction between Cell Division and Circadian Clocks

Our dynamic single-cell recordings have revealed that circadian gene expression persists in daughter cells after cell division. Interestingly, however, cell division can phase shift the circadian cycle. We offer a plausible explanation for this observation in Figure 7E. PER and CRY proteins are the major constituents of the rhythm-generating feedback loop and are thus likely to be state variables whose concentrations determine the phase of the clock (Bae et al., 2001; Kume et al., 1999; van der Horst et al., 1999; Zheng et al., 2001). Hence, cell division most likely influences the clock by affecting the concentration of PER-CRY complexes. We did not determine the accumulation profile of the PER-CRY complexes in these experiments, but we know from previously published experiments (Preitner et al., 2002) that it is antiphasic to that of *rev-erb*α expression (and hence antiphasic to Rev-VNP expression).

Irrespective of when cell division occurs, the arrest of transcription during mitosis and the splitting of cellular components before cytokinesis result in a transient reduction of PER and CRY proteins in the daughter cells. If this reduction occurs during the rising phase of PER and CRY accumulation, the duration required to reach the threshold levels necessary for autorepression will be prolonged and the circadian cycle length increased. In contrast, a reduction of CRY and PER proteins during the descending phase of their accumulation will accelerate the cycle following cell division since the minimal concentrations of these repressor proteins is attained more rapidly.

We were surprised to find that cell division frequency, when plotted against circadian time, appears to follow a highly nonrandom distribution with three peaks spaced roughly by 8 hr. A circadian gating of mitosis to a single time window has recently been demonstrated during liver regeneration following partial hepatectomy (Matsuo et al., 2003). In this case mitosis was probably controlled by the circadian expression of Wee1, a crucial cell cycle regulator. Multiple parameters could account for the different circadian gating of cell division in regenerating liver, in which mitosis is observed during a single time window, and fibroblast cultures, in which mitosis appears to occur during three time windows. For example, it is conceivable that systemic in addition to cell-autonomous circadian signals may restrict the timing of mitosis during hepatic regeneration.

A circadian gating of the S phase has been demonstrated for several proliferative mammalian tissues, such as oral and intestinal epithelia (Bjarnason and Jordan, 2002; Bjarnason et al., 1999), bone marrow (Smaaland et al., 2002), and pancreas (Biederbick and Elsasser, 1998), and for zebrafish embryos and cell lines (Dekens et al., 2003). The purpose, if any, of circadian cell cycle gating is not clear since morphogenesis and tissue homeostasis appear to be normal in genetically arrhythmic animals. However, small selective advantages that are nevertheless important during evolution can readily escape detection in the laboratory.

In conclusion, this study lends strong support to the view that circadian oscillators in cultured fibroblasts are as robust as those operative in SCN neurons. We are aware of the limitations of this simple in vitro system, but we are confident that it will provide valuable assistance in the discovery of novel clock components, in the mechanistic dissection of the circadian clockwork circuitry, and in studying the interactions between the circadian oscillator and the cell division clock.

Experimental Procedures

Real-Time Bioluminescence Monitoring

The construction of the Bmal1-luciferase expression plasmid is described in detail in Supplemental Data online. NIH3T3 cells and Rat-1 cells were transfected with linearized pBmal1-Luc-3′UTR and pIRES-Neo (Clontech) and neomycin-resistant clones were isolated by standard procedure. The resulting cell lines, NIH3T3-Bmal1-Luc-1 and Rat-1-Bmal1-Luc, were maintained in Dulbecco's modified Eagle's medium supplemented with 10% or 5% FCS, respectively, and 200 μg/ml G418, unless otherwise indicated.

Cells were stimulated with either 50% horse serum or 100 nM dexamethasone as described previously (Balsalobre et al., 2000a) with some minor modifications. Briefly, for the stimulation of contact-inhibited cells, 2×10^5 cells were plated into 35 mm culture dishes 4 days before the stimuli were applied. One day before stimulation, the medium was changed to fresh DMEM medium containing 0.5% to 20% FCS, depending on the purpose of the experiment. To stimulate proliferating cells, 2×10^4 cells were plated 2 days before stimulation, and 1 day before the stimulation the medium was changed to fresh DMEM medium containing 5%–20% FCS. After the stimulation, medium was replaced with phenol red-free DMEM supplemented with 20 mM Hepes-NaOH, pH 7.3, 0.1 mM luciferin, and 0.5%–20% FCS. Cultures were maintained at 37°C in a light-tight incubator and bioluminescence was monitored continuously using Hamamatsu photomultiplier tube (PMT) detector assemblies as reported previously (Yamazaki et al., 2000; Yoo et al., 2004). Photon counts were integrated over 1-min intervals.

Fluorescence Timelapse Microscopy and Data Analysis

The construction of the Rev-VNP expression plasmid is described in detail in Supplemental Data. NIH3T3 fibroblasts were transfected

with the Rev-VNP reporter plasmid and pIRES-Neo (Clontech) and neomycin-resistant clones were isolated by standard procedure. The cells were maintained in DMEM supplemented with 10% FCS and 200 μg/ml G418.

NIH3T3-Rev-VNP-1 cells were plated in 35-mm glass bottom dishes (WillCo-dish, type 3522, WillCo Wells B.V.). After stimulating the cells with horse serum or dexamethasone, the medium was replaced by 2 ml phenol red-free DMEM supplemented with 0.5%–20% FCS depending on the experiments. For the experiment without synchronization (Figure 2), 2×10^4 cells were plated directly in 2 ml phenol red-free DMEM supplemented with 20% FCS in a WillCo-dish. The cultures were placed in a 37°C chamber equilibrated with humidified air containing 5% CO_2 throughout the microscopy. Time-lapse microscopy was performed with a Leica AS MDW microscope using a 10× objective. The cells were illuminated every 30 min for 430 ms (excitation at 505 nm) and timelapse series of 5 z-stacks with a 3.0 um step size were captured with the use of a CFP/YFP filter set. DIC images of the same frames were also captured to examine cell morphology. The movies were created from the time-lapse series using Leica AS MDW software.

The fluorescent images were subjected to the data analysis as follows. The sum projection images were constructed from individual z-slices using Image J software. The sum projections were subjected to the fluorescence measurements using MetaMorph software (UIC). The individual fluorescent nuclei were identified manually, and the centers of the fluorescent regions (i.e., centers of the nuclei) were followed manually throughout the timelapse series. Then, the region of interest (ROI) was defined to cover all the fluorescence in the same cell from the first to the last frames, and the fluorescence intensity in the given ROI was measured. The background value/area (BG) was taken as the average intensity of three regions without nuclei, and the sum of background value was obtained by multiplying BG by the area of ROI. The total intensity per nucleus was obtained by subtracting the sum of background from the integrated intensity in a ROI.

Preparation of Mouse Primary Fibroblasts

mPer1$^{-/-}$ single knockout and *mPer1*$^{-/-}$*;mPer2*$^{-/-}$ double knockout mice were generously provided by U. Albrecht (University of Fribourg) (Zheng et al., 2001). MEF cultures were established from day 12 embryos. After heads and livers were removed, the remaining tissue was digested with 0.2% trypsin in PBS for 30 min at room temperature. Digestion was stopped by adding FCS, and the dissociated cells were plated in DMEM containing 10% FCS. The medium was changed the next day and cells were allowed to grow to confluence. After reaching confluence, cells were split 1:3 and used for experiments until passage 10.

To establish mouse primary fibroblasts from adult mice, ears from sacrificed mice were minced and digested with 1 mg/ml collagenase type IA (Sigma) in DMEM with 20% FCS at 37°C overnight. The dissociated cells were washed, plated in fresh medium, and allowed to adhere to the dish for 48 hr. Adhered cells were washed with PBS and grown to 80% confluence in fresh medium. The culture was then split 1:3 at each passage.

Mathematical Models for Populations of Oscillators

Model definition for the analysis of bioluminescence cycles:

This stochastic model describes the luciferase signal emitted by a finite population of oscillators, initially N,

$$s(t) = A\sum_{i=1}^{N} (Be^{-t/T}\cos(2\pi f_i t + \phi) + 1)\theta(t_i^{death} - t)$$

which die abruptly after t_i^{death} (θ is the step function that takes a value 0 for negative argument and 1 otherwise). The death times t_i^{death} are drawn from an exponential distribution with a fixed half-life $t_{1/2}^{death}$. The cellular oscillators are damped cosines initially synchronized to the phase ϕ at time $t = 0$. The damping rate is given by $1/T$ and takes the value 0 for sustained oscillators (as in Figure 3E). The frequencies of the cells are taken constant in time, but each cell has a frequency f_i drawn from a Gaussian with mean $\bar{f}$ and standard deviation σ_f. The constant B is restricted to the interval [0,1] and determines the amplitude of the oscillation relative to a steady state of 1. A is an overall constant and assumes equal amplitude of oscillations for each cell.

Under the approximation that cells die continuously, which is accurate for a large number of cells, the detrended variable

$$Z(t) = \frac{s(t) - AN(t)}{AN(t)} \text{ with } N(t) = Ne^{-\frac{\ln 2t}{t_{1/2}^{death}}}$$

introduced in Figure 3 reduces to

$$Z(t) = \frac{B}{N}\sum_{i=1}^{N} e^{-t/T}\cos(2\pi f_i t + \phi)$$

and takes values in the interval [−1,1]. For an infinite population of cells, Z can be computed analytically and evaluates to

$$Z_\infty(t) = B\cos(2\pi\bar{f}t + \phi)\, e^{-\frac{(2\pi)^2\sigma_f^2 t^2}{2}} e^{-\frac{t}{T}}$$

which is the product of a an oscillation at the mean frequency $\bar{f}$ and an envelope consisting of the product of a Gaussian (the dephasing) and an exponential (the damping). The form of the envelope is used to determine the parameters B, T, σ_f in Figures 3D–3F.

For a finite population, the long-time behavior of $Z(t)$ is different for each new simulation of the random population. Therefore ensemble properties would have to be computed, which is a major mathematical challenge. Here, we exploit the property that the short-time behavior is independent of population size to fit parameters from a single experiment.

Gaussian Mixtures and Model Selection

The Gaussian mixture models used in Figures 1E, 6E, and 7A were obtained using the Mclust package in R (http://www.r-project.org). To gain confidence about the three Gaussian components predicted by Mclust in Figure 6E (Mclust applies the standard BIC, or Bayesian Information Criteria), bootstrap parameter estimates showed well-separated peak locations for up to three components. Finally, a log-likelihood ratio test based on resampling from two-component and three-component fitted models showed that the data support departure from two to three peaks ($p < 0.0005$) but not from three to four ($p = 0.55$).

Acknowledgments

We are grateful to Atsushi Miyawaki, Yosuke Matsuoka, and Francois Spitz for their generous gifts of plasmids and to U. Albrecht for providing *mPer1* and *Per1*; *Per2* mutant mice. We thank Jorge Ritz for technical assistance, N. Roggli for the artwork, and S. Brown, C. Dibner, and N. Preitner for helpful comments on the manuscript. This research was supported by the Swiss National Science Foundation through an individual grant to U.S. and the NCCR programs Frontiers in Genetics (U.S.) and Molecular Oncology (F.N.), the State of Geneva, the Swiss Institute for Experimental Cancer Research (ISREC), the Bonnizzi Theler Stiftung, and the Louis Jeantet Foundation of Medicine.

Received: August 5, 2004
Revised: September 22, 2004
Accepted: October 25, 2004
Published: November 23, 2004

References

Akashi, M., and Nishida, E. (2000). Involvement of the MAP kinase cascade in resetting of the mammalian circadian clock. Genes Dev. *14*, 645–649.

Bae, K., Jin, X., Maywood, E.S., Hastings, M.H., Reppert, S.M., and Weaver, D.R. (2001). Differential functions of mPer1, mPer2, and mPer3 in the SCN circadian clock. Neuron *30*, 525–536.

Balsalobre, A., Damiola, F., and Schibler, U. (1998). A serum shock induces circadian gene expression in mammalian tissue culture cells. Cell *93*, 929–937.

Balsalobre, A., Brown, S.A., Marcacci, L., Tronche, F., Kellendonk, C., Reichardt, H.M., Schutz, G., and Schibler, U. (2000a). Resetting

of circadian time in peripheral tissues by glucocorticoid signaling. Science *289*, 2344–2347.

Balsalobre, A., Marcacci, L., and Schibler, U. (2000b). Multiple signaling pathways elicit circadian gene expression in cultured Rat-1 fibroblasts. Curr. Biol. *10*, 1291–1294.

Biederbick, A., and Elsasser, H. (1998). Diurnal pattern of rat pancreatic acinar cell replication. Cell Tissue Res. *291*, 277–283.

Bjarnason, G.A., and Jordan, R. (2002). Rhythms in human gastrointestinal mucosa and skin. Chronobiol. Int. *19*, 129–140.

Bjarnason, G.A., Jordan, R.C., and Sothern, R.B. (1999). Circadian variation in the expression of cell-cycle proteins in human oral epithelium. Am. J. Pathol. *154*, 613–622.

Brown, S.A., Zumbrunn, G., Fleury-Olela, F., Preitner, N., and Schibler, U. (2002). Rhythms of mammalian body temperature can sustain peripheral circadian clocks. Curr. Biol. *12*, 1574–1583.

Daan, S., and Pittendrigh, C.S. (1976). A functional analysis of circadian pacemakers in nocturnal rodents. IV. Entrainment. J. Comp. Physiol. [A] *106*, 267–290.

Damiola, F., Le Minh, N., Preitner, N., Kornmann, B., Fleury-Olela, F., and Schibler, U. (2000). Restricted feeding uncouples circadian oscillators in peripheral tissues from the central pacemaker in the suprachiasmatic nucleus. Genes Dev. *14*, 2950–2961.

Dekens, M.P., Santoriello, C., Vallone, D., Grassi, G., Whitmore, D., and Foulkes, N.S. (2003). Light regulates the cell cycle in zebrafish. Curr. Biol. *13*, 2051–2057.

Harmar, A.J., Marston, H.M., Shen, S., Spratt, C., West, K.M., Sheward, W.J., Morrison, C.F., Dorin, J.R., Piggins, H.D., Reubi, J.C., et al. (2002). The VPAC(2) receptor is essential for circadian function in the mouse suprachiasmatic nuclei. Cell *109*, 497–508.

Hirota, T., Okano, T., Kokame, K., Shirotani-Ikejima, H., Miyata, T., and Fukada, Y. (2002). Glucose down-regulates Per1 and Per2 mRNA levels and induces circadian gene expression in cultured Rat-1 fibroblasts. J. Biol. Chem. *277*, 44244–44251.

Kume, K., Zylka, M.J., Sriram, S., Shearman, L.P., Weaver, D.R., Jin, X., Maywood, E.S., Hastings, M.H., and Reppert, S.M. (1999). mCRY1 and mCRY2 are essential components of the negative limb of the circadian clock feedback loop. Cell *98*, 193–205.

Le Minh, N., Damiola, F., Tronche, F., Schutz, G., and Schibler, U. (2001). Glucocorticoid hormones inhibit food-induced phase-shifting of peripheral circadian oscillators. EMBO J. *20*, 7128–7136.

Liu, C., Weaver, D.R., Strogatz, S.H., and Reppert, S.M. (1997). Cellular construction of a circadian clock: period determination in the suprachiasmatic nuclei. Cell *91*, 855–860.

Low-Zeddies, S.S., and Takahashi, J.S. (2001). Chimera analysis of the Clock mutation in mice shows that complex cellular integration determines circadian behavior. Cell *105*, 25–42.

Matsuo, T., Yamaguchi, S., Mitsui, S., Emi, A., Shimoda, F., and Okamura, H. (2003). Control mechanism of the circadian clock for timing of cell division in vivo. Science *302*, 255–259.

Mihalcescu, I., Hsing, W., and Leibler, S. (2004). Resilient circadian oscillator revealed in individual cyanobacteria. Nature *430*, 81–85.

Nagai, T., Ibata, K., Park, E.S., Kubota, M., Mikoshiba, K., and Miyawaki, A. (2002). A variant of yellow fluorescent protein with fast and efficient maturation for cell-biological applications. Nat. Biotechnol. *20*, 87–90.

Pando, M.P., Morse, D., Cermakian, N., and Sassone-Corsi, P. (2002). Phenotypic rescue of a peripheral clock genetic defect via SCN hierarchical dominance. Cell *110*, 107–117.

Preitner, N., Damiola, F., Luis Lopez, M., Zakany, J., Duboule, D., Albrecht, U., and Schibler, U. (2002). The orphan nuclear receptor REV-ERBalpha controls circadian transcription within the positive limb of the mammalian circadian oscillator. Cell *110*, 251–260.

Reppert, S.M., and Weaver, D.R. (2002). Coordination of circadian timing in mammals. Nature *418*, 935–941.

Schibler, U., and Sassone-Corsi, P. (2002). A web of circadian pacemakers. Cell *111*, 919–922.

Shen, H., Watanabe, M., Tomasiewicz, H., Rutishauser, U., Magnuson, T., and Glass, J.D. (1997). Role of neural cell adhesion molecule and polysialic acid in mouse circadian clock function. J. Neurosci. *17*, 5221–5229.

Smaaland, R., Sothern, R.B., Laerum, O.D., and Abrahamsen, J.F. (2002). Rhythms in human bone marrow and blood cells. Chronobiol. Int. *19*, 101–127.

Stokkan, K.A., Yamazaki, S., Tei, H., Sakaki, Y., and Menaker, M. (2001). Entrainment of the circadian clock in the liver by feeding. Science *291*, 490–493.

van der Horst, G.T., Muijtjens, M., Kobayashi, K., Takano, R., Kanno, S., Takao, M., de Wit, J., Verkerk, A., Eker, A.P., van Leenen, D., et al. (1999). Mammalian Cry1 and Cry2 are essential for maintenance of circadian rhythms. Nature *398*, 627–630.

Welsh, D.K., Logothetis, D.E., Meister, M., and Reppert, S.M. (1995). Individual neurons dissociated from rat suprachiasmatic nucleus express independently phased circadian firing rhythms. Neuron *14*, 697–706.

Yagita, K., and Okamura, H. (2000). Forskolin induces circadian gene expression of rPer1, rPer2 and dbp in mammalian rat-1 fibroblasts. FEBS Lett. *465*, 79–82.

Yagita, K., Tamanini, F., van Der Horst, G.T., and Okamura, H. (2001). Molecular mechanisms of the biological clock in cultured fibroblasts. Science *292*, 278–281.

Yamaguchi, S., Isejima, H., Matsuo, T., Okura, R., Yagita, K., Kobayashi, M., and Okamura, H. (2003). Synchronization of cellular clocks in the suprachiasmatic nucleus. Science *302*, 1408–1412.

Yamazaki, S., Numano, R., Abe, M., Hida, A., Takahashi, R., Ueda, M., Block, G.D., Sakaki, Y., Menaker, M., and Tei, H. (2000). Resetting central and peripheral circadian oscillators in transgenic rats. Science *288*, 682–685.

Yoo, S.H., Yamazaki, S., Lowrey, P.L., Shimomura, K., Ko, C.H., Buhr, E.D., Siepka, S.M., Hong, H.K., Oh, W.J., Yoo, O.J., et al. (2004). PERIOD2::LUCIFERASE real-time reporting of circadian dynamics reveals persistent circadian oscillations in mouse peripheral tissues. Proc. Natl. Acad. Sci. USA *101*, 5339–5346.

Zheng, B., Albrecht, U., Kaasik, K., Sage, M., Lu, W., Vaishnav, S., Li, Q., Sun, Z.S., Eichele, G., Bradley, A., and Lee, C.C. (2001). Nonredundant roles of the mPer1 and mPer2 genes in the mammalian circadian clock. Cell *105*, 683–694.